New Form of Mixing in Turbulent Sedimentation

Simone Tandurella,[1] Marco Edoardo Rosti,[1,*] Stefano Musacchio,[2] and Guido Boffetta[2]
[1]Complex Fluids and Flows Unit, Okinawa Institute of Science and Technology Graduate University, 1919-1 Tancha, Onna-son, Okinawa 904-0495, Japan
[2]Dipartimento di Fisica and INFN, Università di Torino, via P. Giuria 1, 10125 Torino, Italy

(Received 9 June 2025; accepted 26 January 2026; published 11 March 2026)

We study the sedimentation of finite-size inertial particles in a Rayleigh-Taylor-like setup using state-of-the-art direct numerical simulations. The falling particles are observed to produce two distinct regions: a leading mixing layer with a linear concentration profile followed by a bulk region of uniform density. Unlike classical RT turbulence, the mixing layer extension accelerates with an anomalous, noninteger exponent, while the bulk region moves at a constant velocity. A one-dimensional model based on a local hindered settling law accurately captures the observed dynamics and its dependence on the particle-to-fluid density ratio. The present Letter identifies a new regime of convective mixing which develops at the front of particle suspensions in sedimentation processes.

DOI: 10.1103/tc5z-rxcf

Introduction—The problem of sedimentation has a long, rich history [1], and its role in governing the natural world and shaping technical undertakings is well recognized [2–5]. Despite the deep-seated interest, however, the settling of particle collections remains an unsolved, formidable scientific challenge due to the dissipative nature of the fluid, the complex multibody interactions and the emergence of a wide range of scales.

Among the most immediate, and yet still open, questions is that of finding the average settling velocity v of a suspension of solid particles. In fact, as particles settle, volume conservation produces an average upstream fluid motion. This flow and its effects can be locally complex, and the overall sedimentation, when compared to the settling speed v_t of a single particle, may be either hindered [5–7] or enhanced [8]. For a suspension of solid fraction ϕ, this problem is often referred to as that of finding the hindered settling function $f(\phi) = v/v_t$.

The initial distribution of the suspended particles (i.e., large scale spatial changes of ϕ) can also affect the settling function. One particularly relevant setup is that of a particle-laden suspension which sits atop the same clear, unladen fluid. This condition is realized in a variety of natural scenarios [9–11] and it is relevant in the context of riverine outflows, where a sediment rich river can form a hypopycnal flow, i.e., a superficial layer of dispersed sediment overlaid on a body of water [12,13]. The unstable particle-laden layer collapses, forming plumes of particles which feed convective shear layers and eventually turbulence. In spite of the conceptual and practical relevance of the problem, fundamental aspects remain scarcely investigated, with only few experimental [14], theoretical [15], or numerical [16–19] works available mostly in the small inertia, high-dilution regime, where hindered settling effects are comparatively negligible.

In this Letter, we investigate the yet unexplored regime of finite Stokes, finite dilution in the particle-laden Rayleigh-Taylor configuration, focusing our attention on the role of inertia. We use state-of-the-art, high-resolution direct numerical simulations to study the flow produced by the gravitational settling of $O(10^5)$ finite-size heavy particles layered above an otherwise quiescent fluid. We observe the formation of a turbulent mixing layer in the advancing interfacial region with a quasilinear vertical profile of particle concentration, followed by a bulk region in which particle density remains constant in time. At variance with the classical RT phenomenology [20], we find that the evolution of the extension of the mixing layer displays a power-law growth with an anomalous, noninteger exponent. We develop a simple one-dimensional model of the hindered settling function based on known physical ingredients, which is able to capture the main features of the turbulent sedimentation process.

Model and observables—We consider a large number of monodisperse spherical particles settling in a still fluid in the presence of gravity $\mathbf{g} = (0, 0, -g)$. Particles have diameter d_p and density ρ_p larger than that of the fluid ρ_f. The density ratio is $\gamma = \rho_p/\rho_f$. At time $t = 0$ the particles are randomly distributed exclusively in the top half of the domain, with an initial particle volume fraction of ϕ_b.

*Contact author: marco.rosti@oist.jp

Published by the American Physical Society under the terms of the Creative Commons Attribution 4.0 International license. Further distribution of this work must maintain attribution to the author(s) and the published article's title, journal citation, and DOI.

The fluid phase is governed by the Navier-Stokes equations

$$\frac{\partial \mathbf{u}}{\partial t} + \mathbf{u} \cdot \nabla \mathbf{u} = \frac{1}{\rho_f} \boldsymbol{\nabla} p + \nu \nabla^2 \mathbf{u} + \frac{\mathbf{f}^{pf}}{\rho_f}, \tag{1}$$

for the incompressible velocity field $\mathbf{u}(\mathbf{x}, t)$. $\mathbf{f}^{pf}$ represents the coupling with the particles, whose motion is given by the Newton-Euler equations of motion for rigid spheres

$$m_p \frac{d\boldsymbol{v}_p}{dt} = \mathbf{f}_g + \mathbf{f}^{fp} + \mathbf{f}^{pp}, \tag{2}$$

$$I_p \frac{d\boldsymbol{\omega}_p}{dt} = \mathbf{L}^{fp}. \tag{3}$$

Here, $m_p = \rho_p V_p$ is the mass of the particle of volume V_p, $I_p = m_p d_p^2/10$ its moment of inertia, $\boldsymbol{v}_p$ and $\boldsymbol{\omega}_p$ are the particle's translational and rotational velocities, $\mathbf{f}_g = (\gamma - 1)\rho_f V_p \mathbf{g}$ the buoyancy force, $\mathbf{f}^{fp}$ and $\mathbf{L}^{fp}$ are, respectively, the force and torque due to the fluid-particle interaction, obtained as the particle surface integrals of the coupling force density $\mathbf{f}^{pf}$ and its moment with respect to the particle center $\mathbf{r_p} \times \mathbf{f}^{pf}$.

Direct numerical simulations of the Eqs. (1)–(3) are performed using the in-house developed finite-difference solver *Fujin* (see Supplemental Material [21]). The equations are discretized in a vertically elongated domain of size $L_x \times L_y \times L_z$, where $L_x = L_y$ and $L_z = 4L_x$. Periodic boundary conditions are imposed on the horizontal directions (x, y), while no-slip, no-penetration conditions are set on the top and bottom of the domain. Following the system's symmetries, the collective dynamics of the particle ensemble can be described in terms of the vertical profiles of the local volume fraction $\phi(z, t)$ and of the particle vertical velocity $v(z, t)$, averaged over the horizontal planes. The initial condition for our setup then corresponds to $\phi(z, 0) = 0$ for $0 < z < L_z/2$ and $\phi(z, 0) = \phi_b$ for $L_z/2 < z < L_z$, while $v(z, 0) = 0$ in all the domain. We set $= 10^5$ corresponding to $\phi_b \approx 0.10$. We investigate four different values of the particle-to-fluid density ratio $\gamma = 2, 4, 8, 16$. In order to develop a mathematical model for the mixing layer, we performed additional simulations at volume fractions $\phi_b = 0.05$ and $\phi_b = 0.15$.

Figure 1 shows a snapshot of the system partway through its evolution for the $\gamma = 2$ case. At time $t = 0$ particles begin to fall from the upper part of the domain. The motion is however not uniform, and the formation of plume-like structures in the suspension causes particles closer to the interface with free fluid to fall faster. This produces a complex interfacial region in which the fluid becomes turbulent and affects the dynamics of the falling particles.

Figure 2 displays the vertical profile of particle concentration $\phi(z, t)$ for the case $\gamma = 2$ at different times. In spite of the complexity of the dynamics, vertical profile has a relatively simple form with two distinct regions. In the upper part $z_1(t) \le z \le z_2(t)$ (the "bulk") the volume fraction remains uniform and equal to the original value ϕ_b, while in the lower part $z_0(t) \le z \le z_1(t)$ (the "mixing region") the particle-laden phase mixes with the unladen fluid, resulting in a non-uniform concentration developing a close to linear profile. Both the bulk and the mixing regions fall but with different velocities, and therefore the shape of the profile changes in time. Based on these observations, we model the concentration profile with a simple piecewise linear function



FIG. 1. Volumetric rendering of the instantaneous vertical fluid velocity field $v_z(\boldsymbol{x}, t)$ and particle positions at $t \approx 0.17\tau_t$. Upward/downward velocities are shown in blue/orange, more intense for higher magnitudes of v_z. Regions where $v_z \approx 0$ are rendered as transparent.

$$\phi(z, t) = \begin{cases} 0 & z \le z_0 \wedge z > z_2 \\ \phi_b \frac{z - z_0}{z_1 - z_0} & z_0 \le z \le z_1 \\ \phi_b & z_1 \le z \le z_2. \end{cases} \tag{4}$$

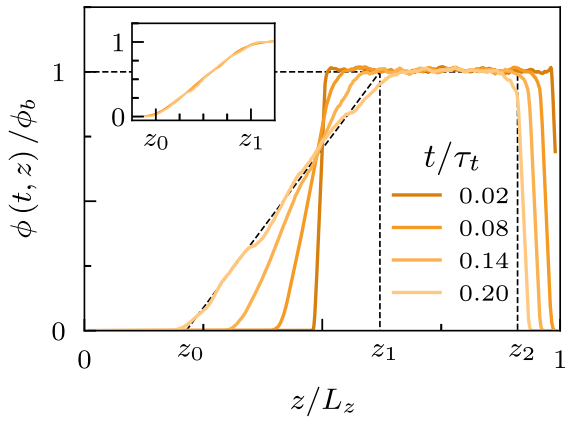


FIG. 2. Particle concentration profiles for the $\gamma = 2$ case at different times. Dashed lines represent the profile model (4) together with the positions of its characteristic points z_0, z_1 and z_2 for the latest time. In the inset, the latest three curves are rescaled according to the instantaneous locations of z_0 and z_1.

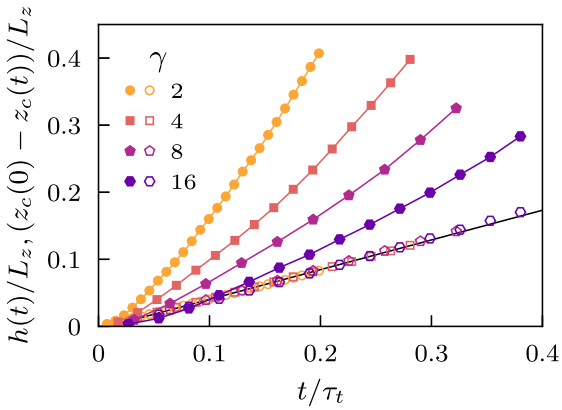


FIG. 3. Time evolution of the width $h(t)$ (filled symbols) and geometric center $z_c(t)$ (empty symbols) of the mixing region for the simulations at different γ. For the geometric center, a black continuous line of slope r is included for guidance.

From the points in (4), we define the extension of the mixing region $h(t) = z_1 - z_0$ and its central point $z_c(t) = (z_1 + z_0)/2$. Volume conservation requires that the distance $z_2 - z_c$ remains constant.

Figure 3 displays the time evolution of the width $h(t)$ and of the center $z_c(t)$ of the mixing region for the four cases at different density ratio. For each run, the values of $z_0(t)$, $z_1(t)$, and $z_2(t)$ are obtained by a fit of the numerical data with the piecewise linear function (4) at the different times. Figure 3 shows that while $z_c(t)$ (and therefore z_2) moves approximately with a constant velocity v_b, proportional to the terminal velocity of a single particle v_t, the growth of $h(t)$ is accelerated with respect to v_t. This effect is strongly dependent on the density ratio, and becomes more important for smaller values of γ.

The different velocities observed in the bulk and mixing regions arise from differences in the suspension local structure. In the bulk of the suspension, where particles remain homogeneously distributed, the particle falling speed is reduced with respect to a single particle because of the change in background flow speed due to the fluid rising homogeneously through the bulk. By comparing the simulations at different volume fractions, we find that, this reduced hindered settling velocity is proportional to ϕ_b, i.e., $v_b \simeq v_t(a - d\phi_b)$ (where a and d are constants of order one independent on γ, see Supplementary material [21]), within the range of parameters explored. This is reminiscent of the Richardson-Zaki (RZ) relation for the hindered settling velocity of Stokesian inertial particles which is valid for small particle Reynolds number Re_p [6]. Inside the mixing region, the particle velocity is not constant, as particles segregate into falling plumes (see Fig. 1), and, as a result, are accelerated by wake effects. This is reflected in the z dependence of the local volume fraction ϕ.

To account for these physical ingredients, we propose a simple 1D model for the evolution of the relative concentration based on mass conservation and its transport by the vertical velocity

$$\frac{\partial \phi}{\partial t} = -\frac{\partial}{\partial z}(v\phi), \tag{5}$$

where v is given by a local hindered model which generalizes the result observed for the bulk region

$$v(z,t) = -v_0(1 - c\phi(z,t)), \tag{6}$$

where v_0 is the velocity of the front position x_0 and $c = (v_0 - v_b)/(v_0\phi_b)$ represents the relative velocity difference between the front and the bulk of particle distribution.

Assuming, as shown by the inset of Fig. 2, that the concentration profile inside the mixing region is a self-similar function $\phi(z,t) = \phi_b f(\tilde{z})$ of the non-dimensional variable $\tilde{z} = (z - z_c(t))/h(t)$, we obtain from (5) and (6) the relation

$$\tilde{z}\frac{dh}{dt} + \frac{dz_c}{dt} = -[v_0 + 2(v_b - v_0)f(\tilde{z})], \tag{7}$$

which shows that $f(\tilde{z})$ must be the linear function $f(\tilde{z}) = 1/2 + \tilde{z}$ in the mixing region $|\tilde{z}| \le 1/2$, which indeed corresponds to the profile (4).

The center of the mixing region moves downward at the same speed of the bulk v_b, while the growth of the mixing region is determined by the difference between the velocity of the front v_0 and of the bulk v_b:

$$\frac{dz_c}{dt} = -v_b, \quad \frac{dh}{dt} = 2(v_0 - v_b). \tag{8}$$

The velocity difference $v_0 - v_b$ is due to the turbulent motions inside the mixing region, the intensity of which depends in

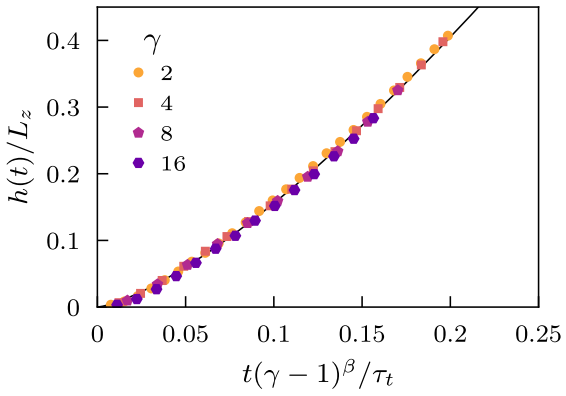


FIG. 4. Time evolution of the width $h(t)$ of the mixing region. Results from different γ are rescaled according to the model (9), which is represented by the black continuous line.

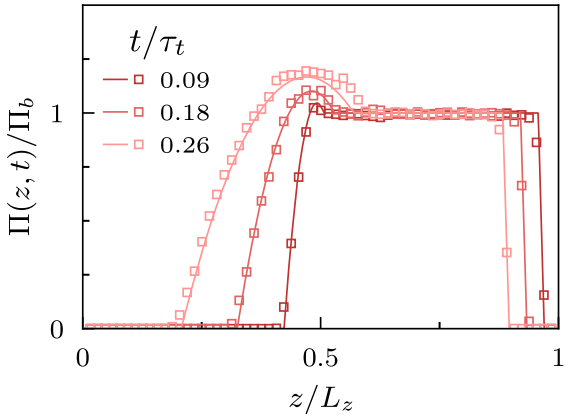


FIG. 5. Vertical profile of the particle flux $\Pi(z,t)$ for the case $\gamma = 4$ at different times. Lines represent the predictions of the theoretical model in the mixing layer given by (11), markers represent the flux according to the simulation data.

general on h and on the density ratio γ. By factorizing this dependence as $v_0 - v_b \propto v_b(\gamma-1)^\beta (h/L_z)^\alpha$, and using the fact that $v_b = rv_t$, we finally obtain the predictions

$$\frac{z_c(t) - z_c(0)}{L_z} = -r\frac{t}{\tau_t}, \quad \frac{h(t)}{L_z} = b\left(\frac{t}{\tau_t}(\gamma-1)^\beta\right)^\xi, \tag{9}$$

where we have introduced the settling time of a single particle $\tau_t = L_z/v_t$, $\xi = 1/(1-\alpha)$, and β and the integration constant b (which depends on the initial volume fraction) are fitting parameters.

We fit the time evolution of $h(t)$ shown in Fig. 3 with the prediction (9). Remarkably, we find the values of the exponent ξ to be independent of γ, and we compute its average value and the error as $\xi = 1.375 \pm 0.015$. We find that all the runs are very well fitted with $\beta = -1/3$, which is therefore fixed, and the coefficient b is obtained as $b = 3.75 \pm 0.10$. Incidentally, we note that the sustained acceleration of the mixing layer expansion ($\xi > 1$) effectively translates into settling enhancement at late times, with v_0 growing up to $1.5v_t$ for case $\gamma = 2$ within the investigated time span.

In Fig. 4 we plot the mixing layer width $h(t)$ rescaled according to the model using the above parameters together with the analytic prediction (9). The remarkable quality of the rescaling indicates that our 1D model is indeed able to capture the complex dynamics of the evolution of particle distribution in a wide range of density ratio. The fact that the exponent β of the density ratio γ is negative reflects quantitatively what observed in Fig. 3, i.e., that the mixing layer is more accelerated with respect to the single particle velocity v_t for lower density ratio. Of course, this behavior cannot be extended to very small values of $\gamma - 1$, because of the divergence of (9) as $\gamma \to 1$. Nonetheless, in the wide range of density ratio investigated by our simulations, the scaling exponent $\beta = -1/3$ is able to describe the observed phenomenology.

The hindered model (5) and (6) allows us to make quantitative predictions for other important quantities, such as the particle flux. This is defined as

$$\Pi(z,t) = -v(z,t)\phi(z,t), \tag{10}$$

and represents the vertical flux of the solid phase. A reference value for this flux is that corresponding to a rigid motion of the bulk of particles with velocity v_b, that is $\Pi_b = v_b\phi_b$. The model prediction for the particle flux in the mixing region $|\tilde{z}| \le 1/2$ has the simple expression in the nondimensional variable $\tilde{z}$,

$$\frac{\Pi(z,t)}{\Pi_b} = \left(\frac{1}{2} + \tilde{z}\right) + \frac{v_0 - v_b}{v_b}\left(\frac{1}{4} - \tilde{z}^2\right), \tag{11}$$

where we remark that both $\tilde{z}$ and v_0 are functions of time.

Figure 5 shows that the prediction (11) reproduces well the numerical vertical flux obtained from our simulations. We remark that no additional parameter is fitted in (11) since all the coefficients are fixed from the time evolution of $h(t)$. A distinctive feature of the particle flux is the presence of a maximum just below the bulk region. This is due to particles accelerated from the lower boundary of the bulk region by the turbulentlike flow in the mixing region and is well captured by the model prediction (11).

Conclusions—We studied the dynamics of a layer of finite-size heavy particles sedimenting in an initially quiescent fluid. In spite of the complexity of the phenomenon, which produces a nonhomogeneous turbulentlike flow, we find that, in the parameter space explored, the particle concentration profile follows a self-similar evolution with a linear mixing layer followed by a bulk region of constant concentration. Due to differences in the local structure of the suspension among the two regions, we

observe both hindrance and enhancement of the average particle settling speeds.

Compared to the classic Rayleigh-Taylor phenomenology, which predicts quadratic scaling for $h(t)$, we find a superlinear but less-than-quadratic power law growth of the mixing layer, with scaling exponent $\xi \approx 1.37$ in the range of parameters investigated. To elucidate the effect of the observed dynamics, we introduce a one-dimensional transport model based on the observation of a RZ-like hindered settling relation within the bulk region, and its further local extension within the mixing layer, which we find justified *a posteriori*. The model is able to explain both the anomalous scaling and its dependence on the density ratio, and is able to accurately predict quantities such as the vertical particle flux. Note that, the standard RT phenomenology is expected in the limit $d_p \to 0$ and $n_p \propto d_p^{-3}$, such that the dynamics of the particles recovers that of Lagrangian tracers and the density difference between the suspension and the pure fluid remains finite. This regime is outside the parameter space explored here.

This Letter represents only a first step in understanding the dynamics of inertial suspensions at large concentrations. Future works will be required to better characterize the fundamental mechanics driving the anomalous mixing layer expansion. Moreover, there would be additional value in further extending our investigation to other regions of the parameter space, as well as comparing with the results of laboratory experiments.

Acknowledgments—The research was supported by the Okinawa Institute of Science and Technology Graduate University (OIST) with subsidy funding to M. E. R. from the Cabinet Office, Government of Japan. M. E. R. also acknowledges funding from the Japan Society for the Promotion of Science (JSPS), Grants No. 24K17210 and No. 24K00810. The authors acknowledge the computer time provided by the Scientific Computing & Data Analysis section of the Core Facilities at OIST, and by HPCI, under the Research Project grant hp250021. S. T. acknowledges A. Chiarini and R. K. Singh for the helpful discussions while preparing this Letter.

Data availability—The data that support the findings of this article are not publicly available upon publication because it is not technically feasible and/or the cost of preparing, depositing, and hosting the data would be prohibitive within the terms of this research project. The data are available from the authors upon reasonable request.

[1] Isaac Newton, De motu fluidorum & resistentia projectilium (Of the motion of fluids, and the resistance made to projected bodies), in *Philosophiae Naturalis Principia Mathematica II* (Royal Society, London, 1687), Sec. VII.

[2] Michael P. Lamb, Jan de Leeuw, Woodward W. Fischer, Andrew J. Moodie, Jeremy G. Venditti, Jeffrey A. Nittrouer, Daniel Haught, and Gary Parker, Mud in rivers transported as flocculated and suspended bed material, Nat. Geosci. **13**, 566 (2020).

[3] Takehiro Koyaguchi, Mark A. Hallworth, Herbert E. Huppert, and R. Stephen J. Sparks, Sedimentation of particles from a convecting fluid, Nature (London) **343**, 447 (1990).

[4] Eckart Meiburg and Ben Kneller, Turbidity currents and their deposits, Annu. Rev. Fluid Mech. **42**, 135 (2010).

[5] Elisabeth Guazzelli and Jeffrey F. Morris, *A Physical Introduction to Suspension Dynamics* (Cambridge University Press, Cambridge, England, 2011), Vol. 45.

[6] J. F. Richardson and W. N. Zaki, The sedimentation of a suspension of uniform spheres under conditions of viscous flow, Chem. Eng. Sci. **3**, 65 (1954).

[7] G. K. Batchelor, Sedimentation in a dilute dispersion of spheres, J. Fluid Mech. **52**, 245 (1972).

[8] Sander G. Huisman, Thomas Barois, Mickaël Bourgoin, Agathe Chouippe, Todor Doychev, Peter Huck, Carla E. Bello Morales, Markus Uhlmann, and Romain Volk, Columnar structure formation of a dilute suspension of settling spherical particles in a quiescent fluid, Phys. Rev. Fluids **1**, 074204 (2016).

[9] Bruce A. Remington, David Arnett, R. Paul Drake, and Hideaki Takabe, Modeling astrophysical phenomena in the laboratory with intense lasers, Science **284**, 1488 (1999).

[10] Hiroki Michioka and Ikuro Sumita, Rayleigh-Taylor instability of a particle packed viscous fluid: Implications for a solidifying magma, Geophys. Res. Lett. **32**, L03309 (2005).

[11] Theodore Green and Teresa Diez, Vertical Plankton transport due to self-induced convection, J. Plankton Res. **17**, 1723 (1995).

[12] Mathew G. Wells and Robert M. Dorrell, Turbulence processes within turbidity currents, Annu. Rev. Fluid Mech. **53**, 59 (2021).

[13] Jeffrey D. Parsons, John W. M. Bush, and James P. M. Syvitski, Hyperpycnal plume formation from riverine outflows with small sediment concentrations, Sedimentology **48**, 465 (2001).

[14] C. Völtz, W. Pesch, and I. Rehberg, Rayleigh-Taylor instability in a sedimenting suspension, Phys. Rev. E **65**, 011404 (2001).

[15] P. Burns and E. Meiburg, Sediment-Laden fresh water above salt water: Linear stability analysis, J. Fluid Mech. **691**, 279 (2012).

[16] Yi-Ju Chou, Fu-Chun Wu, and Wu-Rong Shih, Toward numerical modeling of fine particle suspension using a two-way coupled Euler–Euler model: Part 2: Simulation of particle-induced Rayleigh–Taylor instability, Int. J. Multiphase Flow **64**, 44 (2014).

[17] P. Burns and E. Meiburg, Sediment-Laden fresh water above salt water: Nonlinear simulations, J. Fluid Mech. **762**, 156 (2015).

[18] Xiao Yu, Tian-Jian Hsu, and S. Balachandar, Convective instability in sedimentation: 3-D numerical study, J. Geophys. Res. **119**, 8141 (2014).

[19] Marta Magnani, Stefano Musacchio, and Guido Boffetta, Inertial effects in dusty Rayleigh–Taylor turbulence, J. Fluid Mech. **926**, A23 (2021).

[20] Guido Boffetta and Andrea Mazzino, Incompressible Rayleigh–Taylor turbulence, Annu. Rev. Fluid Mech. **49**, 119 (2017).

[21] See Supplemental Material at http://link.aps.org/supplemental/10.1103/tc5z-rxcf and references therein [22–24] for additional details.

[22] Naoki Hori, Marco E. Rosti, and Shu Takagi, An Eulerian-based immersed boundary method for particle suspensions with implicit lubrication model, Comput. Fluids **236**, 105278 (2022).

[23] Alessandro Chiarini, Ianto Cannon, and Marco Edoardo Rosti, Anisotropic mean flow enhancement and anomalous transport of finite-size spherical particles in turbulent flows, Phys. Rev. Lett. **132**, 054005 (2024).

[24] Alessandro Chiarini, Simone Tandurella, and Marco Edoardo Rosti, Kolmogorov-size particles in homogeneous and isotropic turbulence, J. Fluid Mech. **1007**, A81 (2025).